TIGHTLY COUPLED INDOOR POSITIONING USING UWB/MMWAVE RADAR/IMU

Haiyun Yao, Xiaochen Wang, Hanwen Qi, Xinlian Liang*

State Key Laboratory of Information Engineering in Surveying, Mapping and Remote Sensing, Wuhan University, Luoyu Road NO.129, Wuhan, China - (yaohaiyun, xchwang, hanwenqi, xinlian.liang)@whu.edu.cn

Commission III, WG III/1

KEY WORDS: UWB positioning, Millimeter wave radar, tight coupling, fusion positioning, extended Kalman filter, inertial navigation systems.

ABSTRACT:

The ultra-wideband (UWB)-based positioning has a wide internet of things applications such as smart medical and smart logistics, due to its high positioning accuracy. However, non-line-of-sight radio propagation degrades UWB positioning accuracy. The inertial measurement unit (IMU) can achieve positioning with high accuracy in a short time. In addition, the millimeter wave (mmWave) radar can work well in scenes such as fog, smoke, dust, and other small particles due to the longer wavelength of mmWave Radar, but the drift error of IMU and mmWave radar are all increased rapidly over time. This paper achieves the tight coupling of UWB and IMU, UWB and mmWave radar based on the extended Kalman filter, respectively. The field experiments were conducted based on a handheld platform in an indoor scene to evaluate and compare the performance of the fusion position systems; the experiment results demonstrated that the positioning accuracy by fusing UWB/IMU and UWB/mmWave was significantly higher than that of the positioning using a single sensor.

1. INTRODUCTION

High precision and robust positioning solutions play an indispensable role in the internet of things (IoT) applications such as intelligent transportation, logistics, medical care, and mobile robots. An essential prerequisite for the IoT is knowing the position of each object. For example, the first thing that needs to be solved when multiple mobile robots work together is the precise positioning of each mobile robot itself. Only then is it possible to execute other tasks such as path planning, decision-making, map construction, environment sensing, and collaborative work. The global navigation satellite system (GNSS) can provide high-precision positioning and navigation services for users in outdoor open areas, such as in the application of vehicle positioning and navigation (Zhu, Yang, Xu, Yang, & Zhou, 2022). However, the GNSS cannot provide navigation and positioning services in urban canyons, indoor and other GNSS denied environments.

In recent years, the ultra-wideband (UWB) positioning has received extensive attention from academia and industry due to its high-precision positioning capability. The UWB becomes an effective positioning sensor in GNSS-denied environments. Since the Federal Communications Commission of the United States decided in 2002 to open for UWB to use the band from 3.1 GHz to 10.6 GHz and 22 GHz to 29 GHz (Commission 2002), UWB positioning technology has developed rapidly. It is robust against multipath interference and has great potential for high ranging accuracy(Fontana 2004). Under the line-of-sight (LOS) condition, UWB can achieve centimeter-level positioning accuracy due to its short pulse interval and high time resolution (Cheng and Zhou 2019). However, UWB is very susceptible to non-line-of-sight (NLOS) effects in complex environments such as indoors, leading to a sharp decline in positioning accuracy. Nevertheless, the UWB positioning error does not drift over time.

The strap-down inertial navigation systems (SINSs) based on the inertial measurement unit (IMU) do not require base stations for navigation and positioning so it is flexible. Furthermore, with the rapid development of the low-cost micro-electromechanical systems (MEMS) IMU, the performance of the SINS using the MEMS-IMUs has greatly improved and provides plentiful navigation information such as position, attitude, and speed. The MEMS-IMUs has become a mainstay in many positioning solutions. The SINS with the advantages of fast update frequency and high positioning accuracy in a short time (Zhuang et al. 2019), and therefore is widely used in mobile robot navigation (Iocchi and Pellegrini 2007), indoor pedestrian navigation(Zhuang et al. 2019), and for unmanned drones(You et al. 2020), but SINS errors accumulate rapidly over time.

The millimeter wave (mmWave) radar is robust for the interference of fog, smoke, dust, and other small particles owing to the longer wavelength of mmWave (Lu, Rosa, et al. 2020). Thus, mmWave radar is more suitable for various hostile environments than optical cameras and LiDAR. Further, mmWave radar does not need to pre-deploy external facilities like the anchors in the environment, which is more flexible than those positioning methods that need deploy anchors such as WIFI, or UWB. At present, the fifth generation (5G) mobile communication has been deployed on a large scale. 5G introduces a series of new features, including signals with large bandwidth, ultra-dense networks and large-scale antenna arrays, which are feasible to achieve sub-meter positioning accuarcy indoors (Chen et al. 2021). However, the method is still based on the base stations deployed beforehand.

Although mmWave radar has its advantages, the point cloud data collected by mmWave radar is noisy and sparsity that results in low positioning accuracy. The mmWave radar achieves a positioning accuracy of about 2.5 m indoors based on deep learning (Lu, Saputra, et al. 2020). Notably, the drift

error of mmWave radar will increase rapidly with the distance of increased.

Information fusion of UWB, IMU, and mmWave radar is a feasible means to obtain robust positioning solutions. Currently, a large number of articles have reported studies on the fusion of UWB and IMU using an extended Kalman filter (EKF). EKF can effectively realize the fusion of UWB and IMU positioning (Yao et al. 2017), which showed the fusion accuracy higher than that of the UWB and IMU alone. Feng et al. (Feng et al. 2020) published work on loosely coupled UWB and IMU using the EKF, the positioning accuracy can be reached centimeter-level in line-of-sight condition. In addition, the fusion cases of mmWave and IMU were reported to achieve the positioning of the ground robot (Lu, Saputra, et al. 2020), and ego-velocity estimation in visually degraded environments (Kramer et al. 2020). According to the reporting, the positioning accuracy of fusion of the mmWave and IMU can be reach accuracy at around 1 m.

At present, to the best of our knowledge, the fusion of UWB and mmWave radar has not been reported. In this paper, we realized the fusion of UWB and mmWave radar by EKF tightly coupling. Moreover, we compared the fusion performance of the UWB and mmWave to that of the fusion of the UWB and IMU. The experiments were conducted based on a handheld platform in an indoor scenario to evaluate the effectiveness of our proposed methods, the experimental results show that our proposed methods not only can effectively suppress the NLOS stem from the UWB positioning but also reduce the mmWave and IMU drift error.

2. METHODOLOGY

In this section, we firstly present an overview of fusion positioning systems for the UWB and mmWave radar, UWB and IMU, respectively. The method for positioning using UWB and the SINS algorithm based on the IMU sensor and the data fusion model of the positioning system are introduced.

2.1 System overview

The two fusion positioning systems are achieved by EKF tightly coupling. The structure of the systems is shown in the block diagram in Figure 1 and Figure 2.

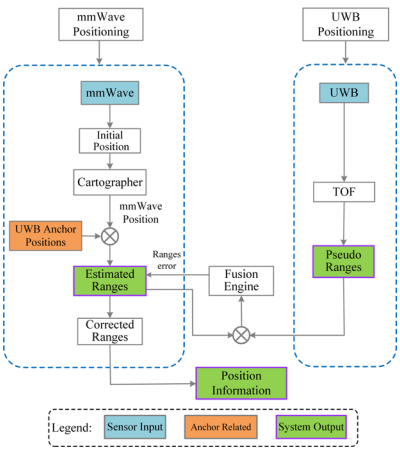

Figure 1. Block diagram of the fusion positioning system of the UWB and mmWave using the EKF tightly coupling.

According to Figure 1 and Figure 2, the fusion positioning systems are composed of three modules. In the fusion of UWB

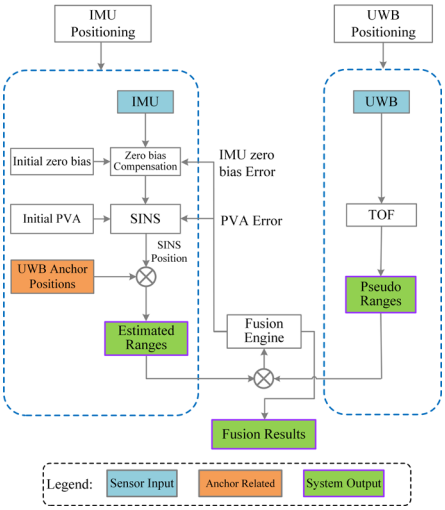

Figure 2. Block diagram of the fusion positioning system of the UWB and IMU using the EKF tightly coupling.

and mmWave, the mmWave positioning subsystem is implemented using Cartographer (Hess et al. 2016), which is an excellent open-source algorithm; the UWB positioning subsystem uses the time of flight (TOF) to calculate the pseudo ranges between the UWB anchors and UWB tag; the fusion engine based on the EKF. The system error state model is the distance error between UWB anchors and tag. The system measurement model is the difference between the estimated ranges and pseudo ranges calculated by the TOF. The optimal state estimate after filtering will feedback the estimated range between the UWB anchors and mmWave radar as shown in Figure 1. The corrected range estimation is used to solve the final position information by least square.

In the fusion of UWB and IMU, the IMU positioning subsystem is implemented using a SINS algorithm, other modules are the same as the fusion of UWB and mmWave. In the SINS positioning subsystem, the real-time position, velocity, and attitude (PVA) of the IMU are obtained by the SINS algorithm under the given initial IMU PVA, acceleration, and gyroscope zero bias. The range between the UWB anchors and IMU can be estimated in real-time by using the anchor coordinates and the current IMU position. In the fusion engine, the system model is realized based on the SINS algorithm, and the difference between the estimated ranges and PRs is the measurement model. After that, the real-time estimated PVA error, acceleration, and gyroscope zero bias will be fed back to the SINS, and the final fusion result will be obtained through the error feedback method.

2.2 UWB positioning based on the TOF

The first step in UWB positioning is to measure the distance between the UWB anchors and the UWB tag, and then calculate the position of the UWB tag based on the measured distance. Common methods of distance measurement include the time of arrival (TOA) (Cetin et al. 2012; Wenyan et al. 2012; Choi, La, and Lee 2018), time difference of arrival (TDOA) (Choi, La, and Lee 2018; Cheng and Zhou 2019), and calculation based on TOF (Neirynck, Luk, and Mclaughlin 2016; Shi et al. 2019). In this paper, the TOF method is selected to calculate the distance

between anchors and tags, since the TOF method does not require anchors and tag clock synchronization, not like the TOA and TDOA; it is a simple and easy-to-operate method with high ranging accuracy. For the specific principle of TOF calculation distance, please refer to the research (Neirynck, Luk, and Mclaughlin 2016).

After the distance between tag and anchor is obtained, the UWB tag position ($X_{tag}, Y_{tag}, Z_{tag}$) can be calculated by solving the nonlinear least-square problem (Gao et al. 2009; Yao et al. 2020)

$$\begin{cases} \left(X_{tag}-X_1\right)^2+\left(Y_{tag}-Y_1\right)^2+\left(Z_{tag}-Z_1\right)^2=d_1{}^2 \\ \left(X_{tag}-X_2\right)^2+\left(Y_{tag}-Y_2\right)^2+\left(Z_{tag}-Z_2\right)^2=d_2{}^2 \\ \vdots \\ \left(X_{tag}-X_m\right)^2+\left(Y_{tag}-Y_m\right)^2+\left(Z_{tag}-Z_m\right)^2=d_m{}^2 \end{cases} \quad (1)$$

where $\left(X_1,Y_1,Z_1\right),\left(X_2,Y_2,Z_2\right)\ \ldots\ \left(X_m,Y_m,Z_m\right)$ are the coordinates of the UWB anchors, d_1, d_2, … d_m denote the distance calculated by TOF method. Linearizing the Equation (1) based on the Taylor formula at the initial value $\left(X_{tag}{}^0, Y_{tag}{}^0, Z_{tag}{}^0\right)$, one can get:

$$\boldsymbol{y}=\mathbf{A}\Delta\boldsymbol{X}+\boldsymbol{\varepsilon} \quad (2)$$

$$\mathbf{A}=\begin{bmatrix} \dfrac{X_{tag}{}^0-X_1}{d_1{}^0} & \dfrac{Y_{tag}{}^0-Y_1}{d_1{}^0} & \dfrac{Z_{tag}{}^0-Z_1}{d_1{}^0} \\ \vdots & \vdots & \vdots \\ \dfrac{X_{tag}{}^0-X_m}{d_m{}^0} & \dfrac{Y_{tag}{}^0-Y_m}{d_m{}^0} & \dfrac{Z_{tag}{}^0-Z_m}{d_m{}^0} \end{bmatrix},$$

$$d_i{}^0=\sqrt{\left(X_{tag}{}^0-X_m\right)^2+\left(Y_{tag}{}^0-Y_m\right)^2+\left(Z_{tag}{}^0-Z_m\right)^2}\ \ m=1,2,\ldots,M \quad (3)$$

$$\Delta\boldsymbol{X}=\hat{\boldsymbol{X}}-\boldsymbol{X}^0=\begin{bmatrix}\hat{X}\\ \hat{Y}\\ \hat{Z}\end{bmatrix}-\begin{bmatrix}X_{tag}{}^0\\ Y_{tag}{}^0\\ Z_{tag}{}^0\end{bmatrix} \quad (4)$$

$$\boldsymbol{y}=\boldsymbol{d}-\boldsymbol{d}^0 \quad (5)$$

where $\hat{\boldsymbol{X}}$ is the coordinate estimation of the UWB tag, $\mathbf{A}$ denotes the design matrix. Thus, the correction $\Delta\boldsymbol{X}$ can be calculated based on the least-squares residual squared sum minimum criterion as:

$$\Delta\boldsymbol{X}=\left(\mathbf{A}^T\mathbf{A}\right)^{-1}\mathbf{A}^T\boldsymbol{y} \quad (6)$$

The UWB tag estimated coordinate value $\hat{\boldsymbol{X}}$ can be obtained by adding the correction $\Delta\boldsymbol{X}$ and the initial value $\boldsymbol{X}^0$.

2.3 Strap-down inertial navigation systems

The SINS algorithm is based on the classical Newtonian mechanical theory, using the specific force f and angular rate ω integral provided by the IMU accelerometer and gyroscope to calculate the PVA of an object (P. Aggarwal 2010; Noureldin, Karamat, and Georgy 2013). The position, velocity, and attitude of the SINS mechanization update algorithm is as follows (Savage 1998; Noureldin, Karamat, and Georgy 2013; Niu et al. 2021):

$$\begin{cases} \mathbf{R}_{b(k)}^{n(k)}=\mathbf{R}_{n(k-1)}^{n(k)}\mathbf{R}_{b(k-1)}^{n(k-1)}\mathbf{R}_{b(k)}^{b(k-1)} \\ \boldsymbol{v}_k^n=\boldsymbol{v}_{k-1}^n+\Delta\boldsymbol{v}_{f,k}^n+\Delta\boldsymbol{v}_{g/cor,k}^n \\ \boldsymbol{\rho}_k^n=\boldsymbol{\rho}_{k-1}^n+\dfrac{1}{2}\left(\boldsymbol{v}_k^n+\boldsymbol{v}_{k-1}^n\right)dt \end{cases} \quad (7)$$

where $\mathbf{R}_{b(k)}^{n(k)}$ is the direction cosine matrix (DCM) relating the body frame (i.e., b frame) to the navigation frame (i.e., n frame) at k moment. $\mathbf{R}_{n(k-1)}^{n(k)}$ is the DCM that accounts for n frame rotation relative to the inertial space from time k-1 to time k. $\mathbf{R}_{b(k)}^{b(k-1)}$ is the DCM that accounts for b frame rotation relative to the inertial space from time k to time k-1. $\boldsymbol{v}_k^n$ is the velocity in the n frame, dt is the IMU sampling interval; $\Delta\boldsymbol{v}_{f,k}^n$ is the specific force-velocity increment, $\Delta\boldsymbol{v}_{g/cor,k}^n$ is the velocity increment caused by the gravity and Coriolis force; $\boldsymbol{\rho}_k^n$ is the position in the navigation frame (n frame) at k time. A detailed derivation of the SINS algorithm can be found in (Savage 1998; P. Aggarwal 2010; Noureldin, Karamat, and Georgy 2013; Groves and Paul 2015; Niu et al. 2021).

2.4 The data fusion model of the positioning system

The system error state model of fusion system of the UWB and mmWave can be written as follows

$$\delta\boldsymbol{X}=\left[\delta d_1\ \delta d_2\ \delta d_3\ \delta d_4\right] \quad (8)$$

where the $\delta\boldsymbol{X}$ denotes the distance error between the UWB tag and anchors. The state transition matrix $\mathbf{F}_k$ is the identity matrix *diag* (1, 1, 1, 1) in this case.

The system error state model of fusion system of the UWB and IMU can be written as follows

$$\delta\boldsymbol{X}=\left[\delta\boldsymbol{\rho}^{\mathrm{T}}\ \ \delta\boldsymbol{v}^{\mathrm{T}}\ \ \delta\boldsymbol{\varphi}^{\mathrm{T}}\ \ \delta\boldsymbol{b}_a{}^{\mathrm{T}}\ \ \delta\boldsymbol{b}_g{}^{\mathrm{T}}\right]^{\mathrm{T}} \quad (9)$$

where $\boldsymbol{\rho}$, $\boldsymbol{v}$, $\boldsymbol{\varphi}$, $\boldsymbol{b}_a$ and $\boldsymbol{b}_g$ are the PVA, accelerometer biases, and gyroscope biases.

Hence, the linearized state-space system model of the discrete-time process is

$$\delta\boldsymbol{X}_{k+1}=\mathbf{F}_k\delta\boldsymbol{X}_k+\mathbf{G}_k\boldsymbol{\omega}_k\in\mathbb{R}^{15} \quad (10)$$

where $\delta\boldsymbol{X}_{k+1}$ is the predicted error state vector, $\delta\boldsymbol{X}_k$ is the previous error state at time k, $\boldsymbol{\omega}_k$ is the process noise with the

covariance matrix $\mathbf{Q}_k = E\left(\boldsymbol{\omega}_k \boldsymbol{\omega}_k^{\mathrm{T}}\right)$, and $\mathbf{F}_k$ denotes the state transition matrix, $\mathbf{G}_k$ denotes the noise driving matrix.

$$\mathbf{F}_k = \begin{bmatrix} \mathbf{I} & dt\mathbf{I} & 0 & 0 & 0 \\ 0 & \mathbf{I} & dt\left[\mathbf{C}_{b,k}^n \boldsymbol{f}_k^b\right]^{\times} & dt\mathbf{C}_{b,k}^n & 0 \\ 0 & 0 & \mathbf{I} & 0 & -dt\mathbf{C}_{b,k}^n \\ 0 & 0 & 0 & \mathbf{I} & 0 \\ 0 & 0 & 0 & 0 & \mathbf{I} \end{bmatrix} \tag{11}$$

$$\mathbf{G}_k = \begin{bmatrix} 0 & 0 & 0 & 0 \\ dt\mathbf{C}_{b,k}^n & 0 & 0 & 0 \\ 0 & -dt\mathbf{C}_{b,k}^n & 0 & 0 \\ 0 & 0 & dt\mathbf{I} & 0 \\ 0 & 0 & 0 & dt\mathbf{I} \end{bmatrix} \tag{12}$$

where $\mathbf{I}$ and 0 represent the 3×3 identity matrix and 3×3 zero matrices, respectively.

The measurement models of fusion system of the UWB and mmWave can be written as follows

$$\boldsymbol{Z}_k = \| \boldsymbol{P}_m^n - \boldsymbol{P}_{mmWave}^n \| - \boldsymbol{d}_m, \ m = 1,2,\cdots,M \tag{13}$$

where M is the number of currently available UWB anchors, $\boldsymbol{P}_m^n \left(m = 1,2,\cdots,M\right)$ is the coordinates of the UWB anchors in the navigation coordinate, $\boldsymbol{P}_{mmWave}^n$ is the mmWave radar position in n frame at k time, $\boldsymbol{d}_m$ is the distance between UWB tag and anchor calculated by TOF.

The measurement models of the fusion system the UWB and IMU can be expressed as follows

$$\boldsymbol{Z}_k = \| \boldsymbol{P}_m^n - \boldsymbol{P}_{imu}^n \| - \boldsymbol{d}_m, \ m = 1,2,\cdots,M \tag{14}$$

where $\boldsymbol{P}_{imu,k}^n$ is the IMU position in n frame at k time.

By linearizing equation (14), the measurement equation can be written

$$\boldsymbol{Z}_k = \mathbf{H}_k \delta \boldsymbol{X}_k + \boldsymbol{v}_k \tag{15}$$

the $\mathbf{H}_k$ is the Jacobian matrix, which is obtained as

$$\mathbf{H}_k = \begin{bmatrix} \mathbf{J}_{\mathrm{F}} & 0_{M\times3} & 0_{M\times3} & 0_{M\times3} \end{bmatrix} \tag{16}$$

where

$$\mathbf{J}_{\mathrm{F}} = \frac{\boldsymbol{P}_{imu}^n - \boldsymbol{P}_m^n}{\| \boldsymbol{P}_m^n - \boldsymbol{P}_{imu}^n \|} \quad m = 1,2,\cdots,M \tag{17}$$

The detail about EKF algorithms can be found in the literature(Feng et al. 2020).

3. EXPERIMENT AND RESULT

In this section, we conduct experiments in an indoor scene to evaluate the effectiveness of the proposed methods.

3.1 Test site

A meeting room with NLOS conditions due to many tables and chairs was selected as an experimental scene to test the proposed method as shown in Figure 3.

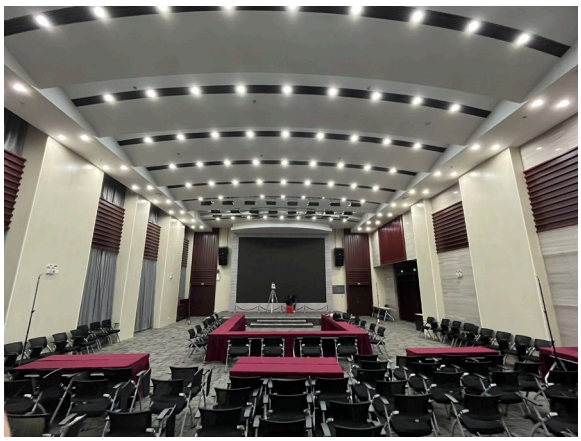

Figure 3. Experimental scene with NLOS conditions.

The equipment used in the experiment is shown in Figure 4. A handheld platform that was equipped with a series of experiment devices such as the UWB tag, mmWave radar and a Leica GRZ4 360° prism was used to conduct the experiment. The on-board computing unit was an Intel NUC computer. The UWB tag was equipped with MPU-6500 low-cost MEMS IMU. The ground truths were collected using a Leica TS60 total station and a GRZ4 360°prism fixed on handheld platform. The GRZ4 360° prism delivers an overall accuracy of 2-5 millimetres.

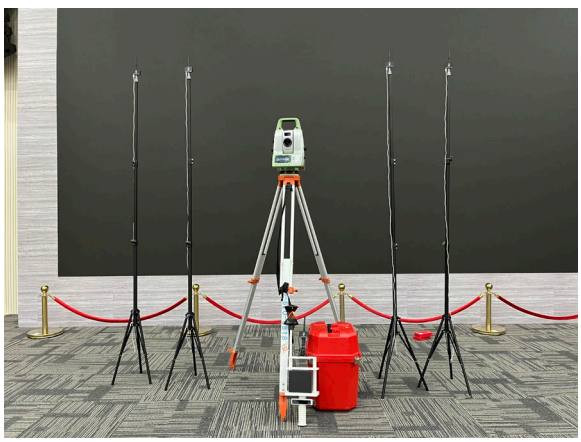

Figure 4. The experiment equipment.

3.2 Result and discussion

The experiment was conducted in an indoor scene to evaluate the effectiveness of the proposed methods. The path length of the experimental test was about 35m, and the experimental

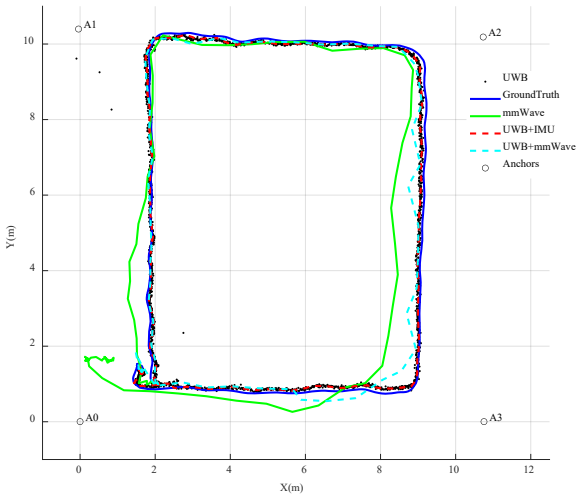

Figure 5. The positioning trajectories of different methods

positioning trajectories of the four algorithms are shown in Figure 5. As shown in Figure 5, the UWB positioning display mutations in local areas due to NLOS, e.g., the black dots far away from all other UWB measurement positions in the up left corner. The EKF tight coupling of UWB and IMU can effectively suppress the adverse effects of NLOS, making the fused trajectory closer to the ground truth. The trajectory of mmWave radar drifted as the path length increased. After using UWB and mmWave radar fusion, it can be seen that the fused trajectory was closer to the ground truth. This shows that the fusion algorithm is effective. The distance information of UWB were used to correct the position calculated by mmWave radar and effectively achieved the fusion positioning.

The positioning errors of the four positioning methods were shown in Figure 6.

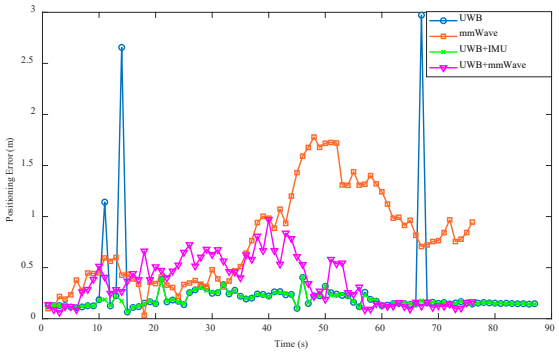

Figure 6. The positioning error of the different positioning methods

According to the Figure 6, there are a few outliers in UWB positioning due to NLOS. The fusion positioning of the UWB and IMU effectively eliminated the outliers and improved the positioning accuracy. Compared with UWB, the positioning error of mmWave radar was larger, and the maximum value exceeded 1.5m. The maximum value was less than 0.8m after the fusion of UWB and mmWave, and the fusion positioning error of UWB and mmWave was significantly reduced.

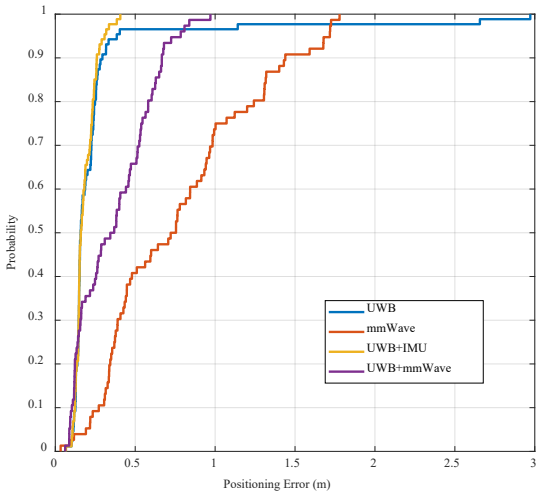

Figure 7. The CDFs of different positioning methods

The cumulative distribution function (CDFs) of positioning errors corresponding to the trajectories in Figure 5 are shown in Figure 7. According to the Figure, the 90% error of the mmWave and UWB+mmWave were 0.67m and 1.439m, respectively, which reduced by 53.44% errors after fusing the UWB and mmWave.

The maximum, mean, and root mean square (RMS) errors were used to evaluate the positioning accuracy. Figure 8 showed the statistics of the different positioning methods. The maximum error of the UWB, mmWave, UWB+IMU, and UWB+mmWave were 2.972m, 1.779m, 0.407m, and 0.970m, respectively. The RMS, mean and maximum error of the UWB were significantly reduced after fusing the UWB and IMU. Similarly, the fusion of UWB and mmWave can also effectively improve positioning accuracy of the mmWave. The RMS error of the UWB, mmWave, UWB+IMU, and UWB+mmWave were 1.18m, 0.905m, 0.195m and 0.443m, respectively, which reduced by 83.47% and 51.05% errors after fusing the UWB and IMU, UWB and mmWave, respectively.

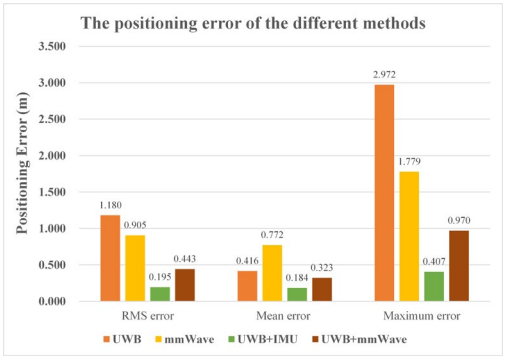

Figure 8. The error statistics of the different positioning methods

The boxplot of the positioning errors of various methods are shown in Figure 9. It can be seen from Figure 9 that the positioning accuracy of the fusion has been improved after fusing of IMU and UWB, especially for the elimination of the UWB positioning outliers. The fusion of the UWB and mmWave can effectively improve the mmWave positioning

accuracy. The experimental results show that the proposed method can effectively realize the fusion of UWB and mmWave, UWB and IMU, respectively.

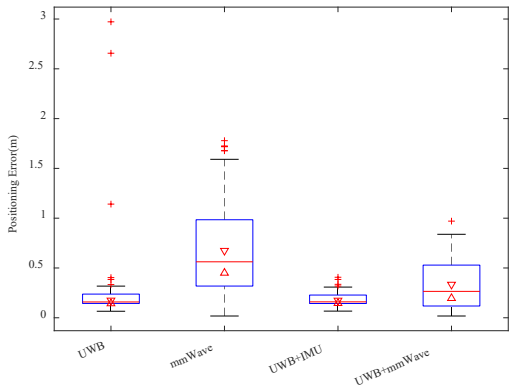

Figure 9. The positioning error of the different positioning method

4. CONCLUSION

Tightly coupling of UWB and mmWave radar, and UWB and IMU were achieved based on EKF in this paper, respectively. The experiments have demonstrated that our proposed methods not only effectively suppress the error accumulation of the IMU and mmWave, but also resist the adverse impact of the non-line-of-sight radio propagation of the UWB positioning. The RMS error of the UWB, mmWave, UWB+IMU, and UWB+mmWave reduced by 83.47% and 51.05% errors after fusing the UWB and IMU, UWB and mmWave, respectively. The 90% error of the mmWave and UWB+mmWave were 0.67m and 1.439m, respectively, which reduced by 53.44% errors after fusing the UWB and mmWave.

ACKNOWLEDGMENTS

The authors would like to acknowledge the financial supports from Natural Science Fund of China (32171789, 32211530031) and Wuhan University (WHUZZJJ202220).

REFERENCES

Cetin, O., H. Nazli, R. Gurcan, H. Ozturk, and H. P. Partal. 2012. "An experimental study of high precision TOA based UWB positioning systems." In *IEEE International Conference on Ultra-wideband*.

Chen, Liang, Xin Zhou, Feifei Chen, Lie-Liang Yang, and Ruizhi Chen. 2021. 'Carrier Phase Ranging for Indoor Positioning with 5G NR Signals', *IEEE Internet of Things Journal*.

Cheng, Yun, and Taoyun Zhou. 2019. "UWB indoor positioning algorithm based on TDOA technology." In *2019 10th international conference on information technology in medicine and education (ITME)*, 777-82. IEEE.

Choi, B., K. La, and S. Lee. 2018. 'UWB TDOA/TOA measurement system with wireless time synchronization and simultaneous tag and anchor positioning', *2018 Ieee International Conference on Computational Intelligence and Virtual Environments for Measurement Systems and Applications (Civemsa)*: 1-6.

Commission, Federal Communications. 2002. "Revision of Part 15 of the Commission's Rules Regarding Ultra-Wideband Transmission Systems." In. Washington, DC, : Federal Communications Commission.

Feng, D. Q., C. Q. Wang, C. L. He, Y. Zhuang, and X. G. Xia. 2020. 'Kalman-Filter-Based Integration of IMU and UWB for High-Accuracy Indoor Positioning and Navigation', *IEEE Internet of Things Journal*, 7: 3133-46.

Fontana, R. J. 2004. 'Recent system applications of short-pulse ultra-wideband (UWB) technology', *Ieee Transactions on Microwave Theory and Techniques*, 52: 2087-104.

Gao, W., G. Kamath, K. Veeramachaneni, and L. Osadciw. 2009. "A particle swarm optimization based multilateration algorithm for UWB sensor network." In *Conference on Electrical & Computer Engineering*.

Groves, and D. Paul. 2015. 'Principles of GNSS, inertial, and multisensor integrated navigation systems, 2nd edition [Book review]', *IEEE Aerospace & Electronic Systems Magazine*, 30: 26-27.

Hess, Wolfgang, Damon Kohler, Holger Rapp, and Daniel Andor. 2016. "Real-time loop closure in 2D LIDAR SLAM." In *2016 IEEE international conference on robotics and automation (ICRA)*, 1271-78. IEEE.

Iocchi, L., and S. Pellegrini. 2007. 'Building 3D maps with semantic elements integrating 2D laser, stereo vision and INS on a mobile robot', *in 2nd ISPRS International Workshop 3D-ARCH*.

Kramer, Andrew, Carl Stahoviak, Angel Santamaria-Navarro, Ali-Akbar Agha-Mohammadi, and Christoffer Heckman. 2020. "Radar-inertial ego-velocity estimation for visually degraded environments." In *2020 IEEE International Conference on Robotics and Automation (ICRA)*, 5739-46. IEEE.

Lu, Chris Xiaoxuan, Stefano Rosa, Peijun Zhao, Bing Wang, Changhao Chen, John A. Stankovic, Niki Trigoni, and Andrew Markham. 2020. "See through smoke: robust indoor mapping with low-cost mmWave radar." In *Proceedings of the 18th International Conference on Mobile Systems, Applications, and Services*, 14–27. Toronto, Ontario, Canada: Association for Computing Machinery.

Lu, Chris Xiaoxuan, Muhamad Risqi U. Saputra, Peijun Zhao, Yasin Almalioglu, Pedro P. B. de Gusmao, Changhao Chen, Ke Sun, Niki Trigoni, and Andrew Markham. 2020. 'milliEgo: single-chip mmWave radar aided egomotion estimation via deep sensor fusion.' in, *Proceedings of the 18th Conference on Embedded Networked Sensor Systems* (Association for Computing Machinery).

Neirynck, D., E. Luk, and M. Mclaughlin. 2016. "An Alternative Double-Sided Two-Way Ranging Method." In *Workshop on Positioning, Naviation and Communications*.

Niu, X. J., T. Liu, J. Kuang, and Y. Li. 2021. 'A Novel Position and Orientation System for Pedestrian Indoor Mobile Mapping System', *IEEE Sensors Journal*, 21: 2104-14.

Noureldin, A., T. B. Karamat, and J. Georgy. 2013. *Fundamentals of Inertial Navigation, Satellite-based Positioning and their Integration*.

P. Aggarwal, Z. Syed and N. El-Sheimy. 2010. *MEMS-based integrated navigation* (Artech House).

Savage, P. G. 1998. 'Strapdown inertial navigation integration algorithm design part 1: Attitude algorithms', *Journal of Guidance Control and Dynamics*, 21: 19-28.

Shi, Q., S. H. Zhao, X. W. Cui, M. Q. Lu, and M. D. Jia. 2019. 'Anchor Self-Localization Algorithm Based on UWB Ranging and Inertial Measurements', *Tsinghua Science and Technology*, 24: 728-37.

Wenyan, Liu, Hong, Ding, Xiaotao, Huang, Zelong, and Liu. 2012. 'TOA Estimation in IR UWB Ranging with Energy Detection Receiver Using Received Signal Characteristics', *Communications Letters IEEE*.

Yao, H. Y., H. Shu, X. L. Liang, H. J. Yan, and H. X. Sun. 2020. 'Integrity Monitoring for Bluetooth Low Energy Beacons RSSI Based Indoor Positioning', *Ieee Access*, 8: 215173-91.

Yao, L., Ywa Wu, L. Yao, and Z. Z. Liao. 2017. "An integrated IMU and UWB sensor based indoor positioning system." In *2017 International Conference on Indoor Positioning and Indoor Navigation (IPIN)*.

You, W. D., F. B. Li, L. Q. Liao, and M. L. Huang. 2020. 'Data Fusion of UWB and IMU Based on Unscented Kalman Filter for Indoor Localization of Quadrotor UAV', *Ieee Access*, 8: 64971-81.

Zhuang, Y., J. Yang, L. Qi, Y. Li, Y. Cao, and N. El-Sheimy. 2019. 'A Pervasive Integration Platform of Low-Cost MEMS Sensors and Wireless Signals for Indoor Localization', *IEEE Internet of Things Journal*, 5: 4616-31.